Electronic Supplementary Material (ESI) for Nanoscale Horizons.

Electronic Supplementary Information

Directional ultrafast charge transfer in a $WSe_2/MoSe_2$ heterostructure selectively probed by time-resolved SHG imaging microscopy

J. E. Zimmermann[1], Y. D. Kim[2,3], J. C. Hone[2], U. Höfer[1], and G. Mette[1,*]

[1]Fachbereich Physik und Zentrum für Materialwissenschaften, Philipps-Universität, 35032 Marburg, Germany

[2]Department of Mechanical Engineering, Columbia University, New York 10027, United States

[3]Present Address: Department of Physics, Kyung Hee University, Seoul 02447, Republic of Korea

* corresponding author: gerson.mette@physik.uni-marburg.de

1 Experimental setup

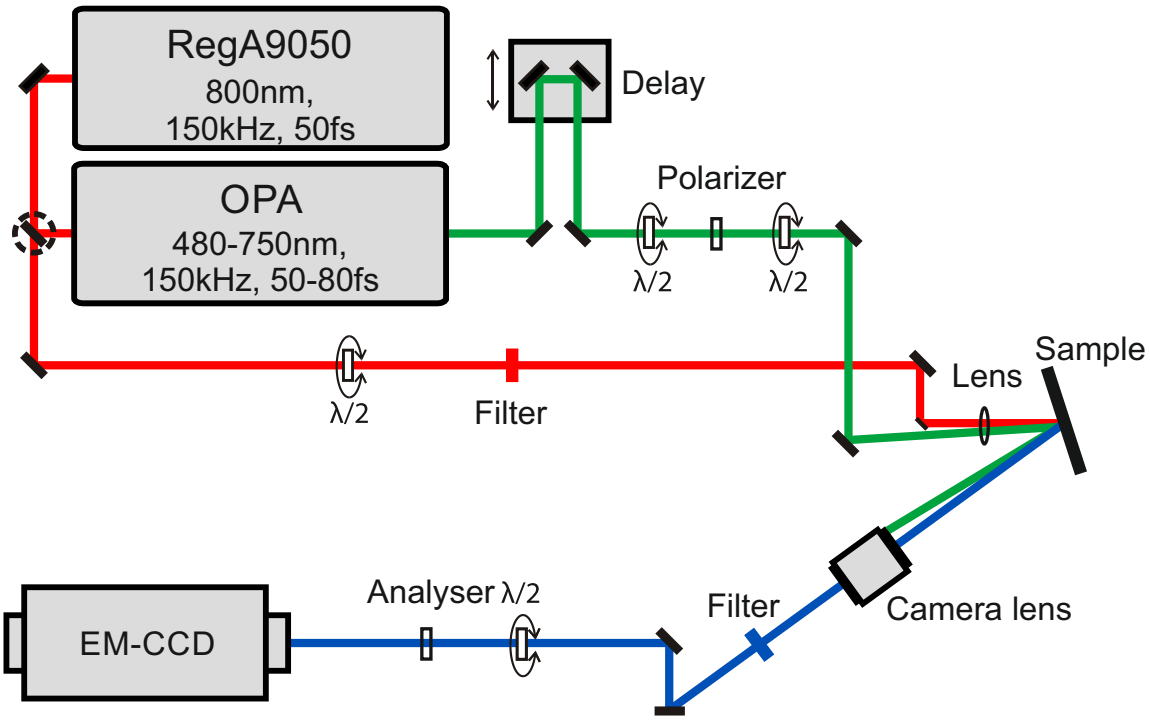

Figure S1: **Experimental setup.** The fs-laser pulses are generated by a Ti:Sapphire laser amplifier system (RegA). The main part of the amplifier output (90 %) is used to pump an optical parametric amplifier (OPA) generating visible pump pulses. The remaining part of the amplifier output is sent through an RG715 filter and then used to probe the SH response. Pump and probe beam are focussed onto the sample nearly collinear under an angle of 18°. The specular reflected SH light of the probe pulse is imaged optically magnified by a camera lens through a FBH400-40 filter onto the CCD camera.

2 Sample characterization

The studied hBN/WSe_2/$MoSe_2$/hBN heterostructure has been characterized in detail by optical spectroscopy in a previous work [1]. Fig. 11(a) of Ref. [1] shows the photoluminescence (PL) spectra of our sample at 300 K and 10 K. At room temperature, the PL spectrum obtained

from the heterostructure can be fitted with the sum of three Gaussian functions representing the A-exciton and trion of WSe_2 and the A-exciton of $MoSe_2$. At low temperature, the biexciton of WSe_2 and the trion of $MoSe_2$ can be observed additionally. Furthermore, PL lifetimes derived from transient photoluminescence are shown in Fig. 14 of Ref. [1] (last column). Raman spectra of the heterostructure at 300 K are given in Fig. 12 of Ref. [1] (sample 6). Three Raman modes are observed which can be attributed to WSe_2 A^1_g and E^1_{2g} and $MoSe_2$ E^1_{2g} modes. These Raman and PL measurements of Ref. [1] confirm that the hBN/WSe_2/$MoSe_2$/hBN heterostructure studied in the present work by time-resolved SHG microscopy represents a heterobilayer of WSe_2 and $MoSe_2$.

In addition, the heterostructure has been characterized by atomic force microscopy (Agilent SPM 5500) operated under ambient conditions in tapping mode. The AFM image and different topographic line scans are shown in Fig. S2.

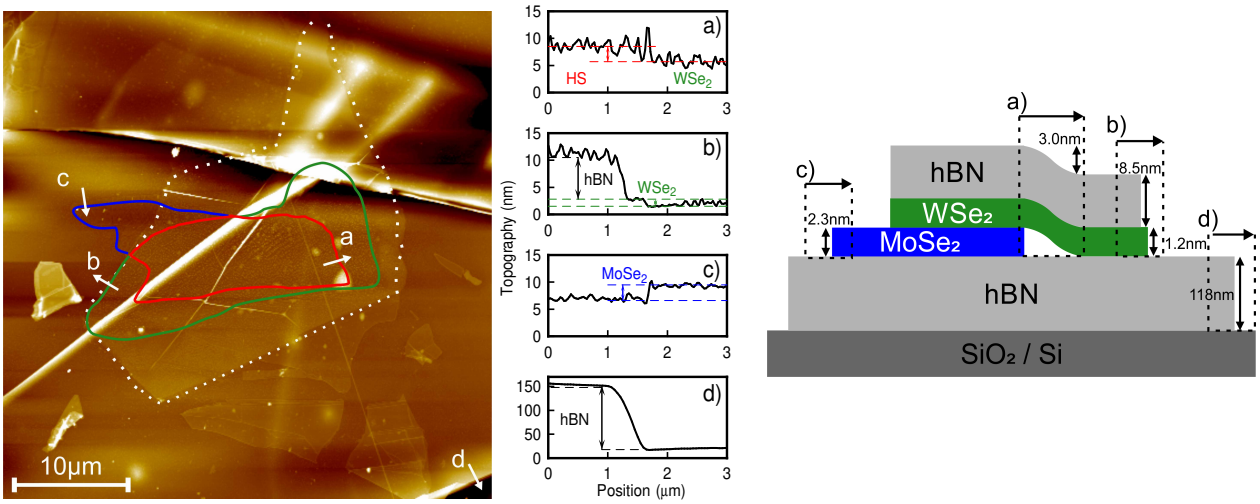

Figure S2: **AFM measurements.** Left: AFM image of the studied hBN/WSe_2/$MoSe_2$/hBN sample with the heterostructure (HS) and the WSe_2 and $MoSe_2$ monolayer regions highlighted by red, green and blue color, respectively. Center: Topographic line scans along the white arrows labelled as (a) - (d) in the AFM image. Right: Schematic side view of the heterostructure illustrating the particular regions of the different line scans and the extracted height differences.

3 Supplemental time-resolved data

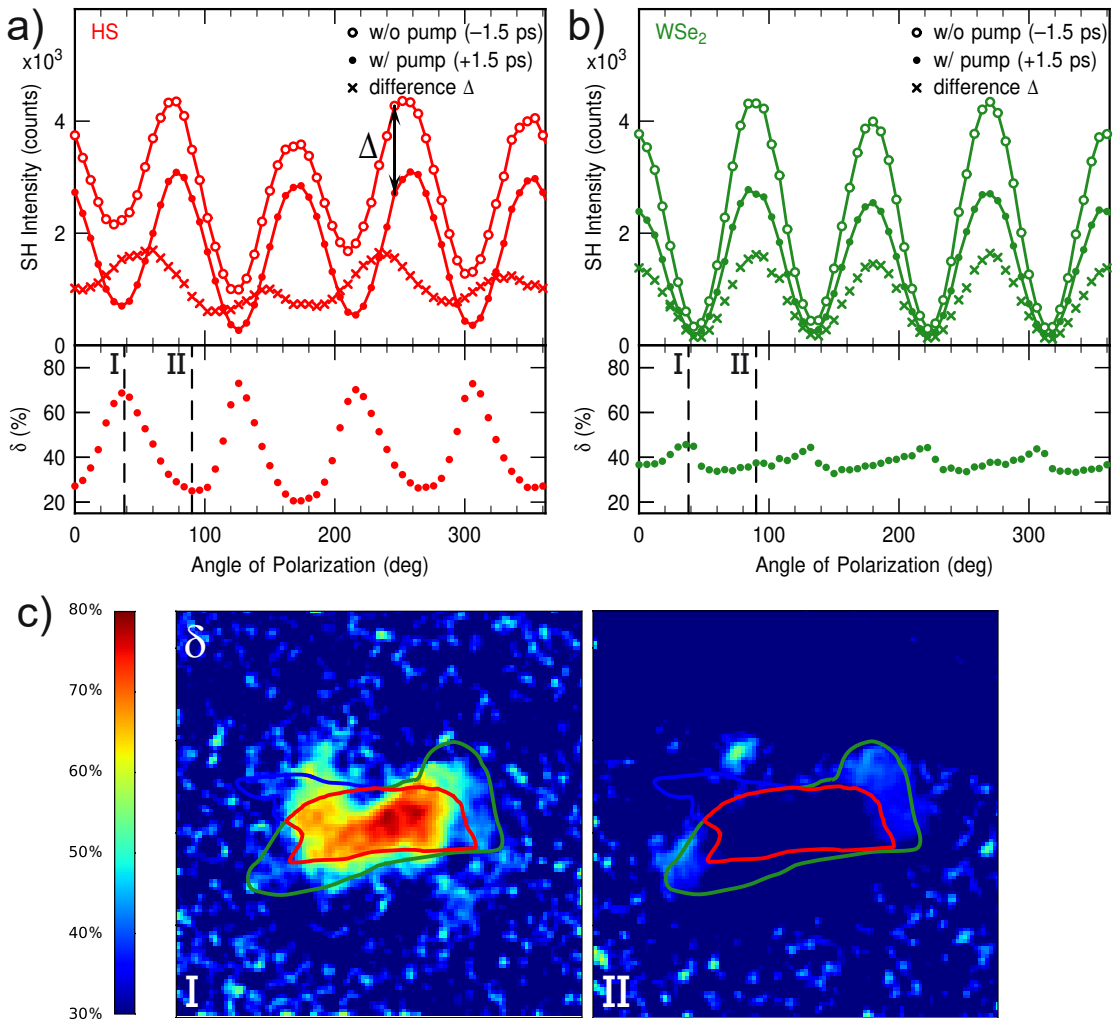

Figure S3: **Polarizational SHG anisotropy upon optical excitation.** (a) Polarization dependent measurements of the SH response obtained from the $WSe_2/MoSe_2$ heterostructure upon 2.09 eV excitation for two different pump-probe delays of -1.5 ps (empty dots) and +1.5 ps (filled dots) as already shown in Fig. 3 of the maintext. The difference of the two data sets (crosses) displays the absolute change of the SH signal (Δ) in dependence of the probe polarization. Dividing the absolute signal change by the SH response at negative delays exhibits a striking anisotropy of the relative change of the SH signal (δ) varying between $\approx$ 20% and $\approx$ 75% of pump-induced decrease. (b) Direct comparison of the corresponding evaluation for the WSe_2 monolayer reveals the absence of the strong anisotropy present in the heterostructure. Instead an almost isotropic pump-induced decrease of $\approx$ 40% is observed. (c) Images of the spatial distribution of δ for two different polarizations (I and II). The strong pump-induced change is clearly localized within the heterostructure region.

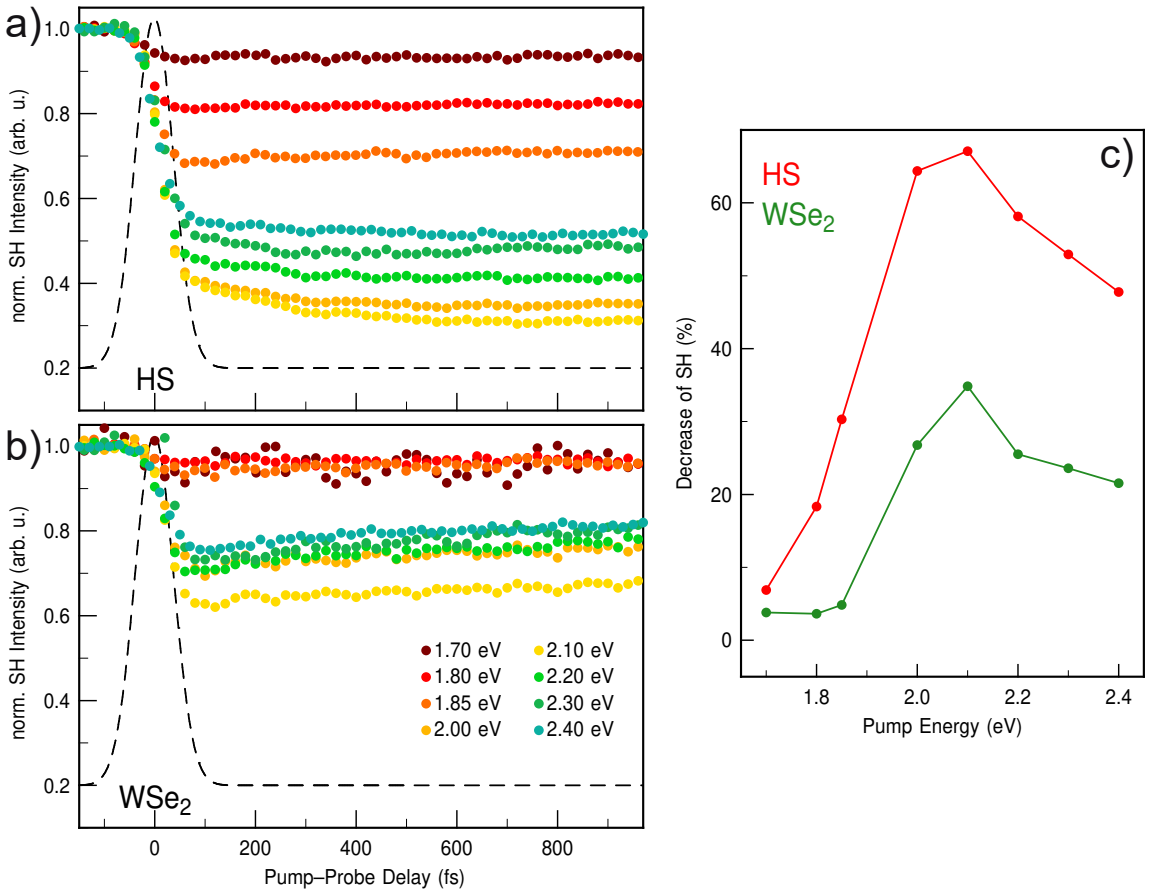

Figure S4: **Time-resolved SHG in dependence of the pump-photon energy.** The pump-photon energy is varied between 1.70 – 2.40 eV, the SH response is measured with probe polarization I most sensitive to the $MoSe_2$ layer. (a) Averaged SH intensities of the heterostructure region in dependence of the pump-probe delay. The cross correlation of the laser pulses corresponds to the black line. (b) Corresponding SH transients of the WSe_2 monolayer region. (c) Extracted decrease of the SH signal in temporal overlap in dependence of the pump-photon energy. For both, the heterostructure and the WSe_2 monolayer, a clear resonant behavior can be observed, which matches well with the B-exciton energy of WSe_2. The SH response of the heterostructure exhibits significant differences compared to the WSe_2 monolayer signal as soon as the threshold energy of 2.00 eV is reached. For pump-photon energies ≥ 2.00 eV, the form of the SH transient changes substantially and reveals a delayed intensity decrease as discussed further in the main text.

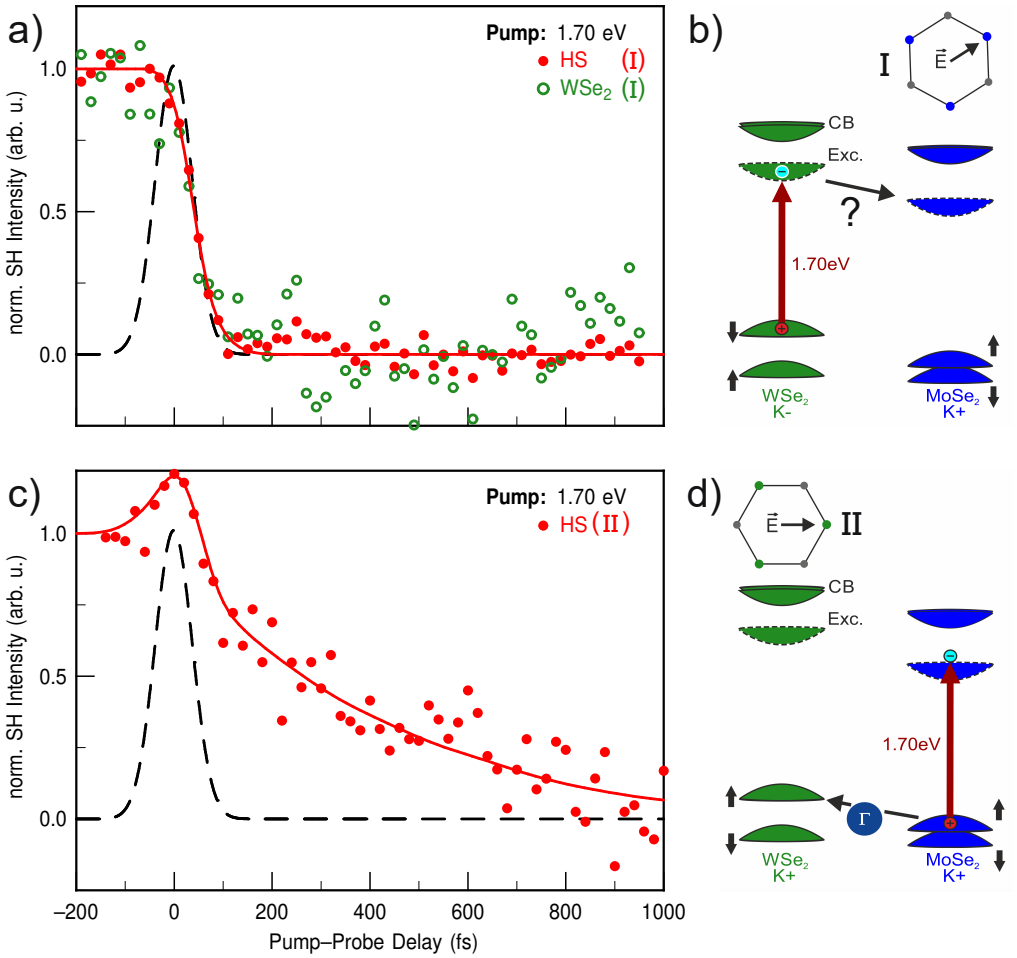

Figure S5: **Time-resolved SHG for photoexcitation with 1.7 eV.** The chosen pump-photon energy is resonant with the WSe_2 A-excitons (1.68 eV) and non-resonant with the $MoSe_2$ A-excitons (1.56 eV). (a) SH transients of the heterostructure (red) in comparison with the respective WSe_2 signal (green) for probe polarization I sensitive to $MoSe_2$. A delayed decrease of the heterostructure signal associated with ultrafast electron transfer from WSe_2 to $MoSe_2$ is not observed. (b) Schematic drawing of the potential electron transfer to $MoSe_2$ after resonant optical excitation of WSe_2 A-excitons. (c) SH transient of the heterostructure as in (a) for probe polarization II sensitive to WSe_2. Direct comparison with the heterostructure signal in a) indicates a delayed decrease due to interlayer hole transfer. (d) Schematic drawing of the hole transfer to WSe_2 after non-resonant optical excitation of $MoSe_2$ A-excitons. Please note, that the noise level of this measurement is comparatively large, since it was performed at the tuning limit of our laser setup. Solid red lines are a guide to the eye. The cross correlation of the laser pulses is shown as a black line. The increase of the SH intensity around temporal overlap for polarization II is caused by an interference of pump and probe beam due to their similar wavelength and polarisation.

4 Rate-equation model for interlayer charge transfer

To describe the relaxation dynamics visible in the SH transients a rate-equation approach is used. Here, a population is generated from two ground states by convolution with the pump pulse. This change in charge-carrier density is then in turn monitored by the probe pulse. For the delayed decrease seen in the heterostructure transients, the energetically higher lying state $|2>$ couples to the lower lying state $|1>$ further filling it with the time constant τ_{transfer}. This repopulation manifests as a further reduction of SH intensity even after the pump pulse has fully subsided as can be seen in Fig. 4 of the main text. The dynamics can therefore be described by:

$$\frac{\mathrm{dN_1}}{\mathrm{dt}} = -\mathrm{N_1}\lambda_1 + \mathrm{N_2}\lambda_{\mathrm{transfer}} \tag{1}$$

where $\mathrm{N_1}$ is the population of state $|1>$, $\mathrm{N_2}$ is the population of state $|2>$ and λ_1 the decay rate of state $|1>$. For an easier understanding Fig. S6 illustrates the transfer process for the example of the $MoSe_2 \rightarrow WSe_2$ hole transfer.

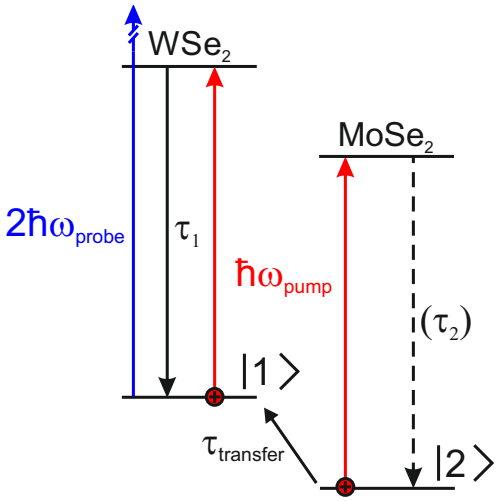

Figure S6: **Illustration of the decay mechanism.** In the shown example $MoSe_2$ is pumped resonantly after which the holes scatter into the VBM of WSe_2. The applied model neglects the decay τ_2 for the excited states in $MoSe_2$ since it occurs on a slower timescale.

References

[1] L. M. Schneider, S. Lippert, J. Kuhnert, O. Ajayi, D. Renaud, S. Firoozabadi, Q. Ngo, R. Guo, Y. D. Kim, W. Heimbrodt, J. C. Hone, and A. Rahimi-Iman, Nano-Structures & Nano-Objects **15**, 84 (2018).